Balanced SSFP-like imaging with simultaneous Water-Fat Separation and Band Reduction using Small-tip Fast Recovery

Feng Zhao[1], Hao Sun[2], Jon-Fredrik Nielsen[1], Jeffrey A Fessler[2], and Douglas C Noll[1]

[1]*Biomedical Engineering, The University of Michigan, Ann Arbor, MI, United States,* [2]*EECS, The University of Michigan, Ann Arbor, MI, United States*

Introduction: Balanced SSFP provides high SNR efficiency and useful T_2/T_1 weighting, but suffers from bright fat signal and off-resonance banding. Recently, a bSSFP-based method was proposed for simultaneous suppressing fat and banding artifacts from two phase-cycled acquisitions [1]. That method requires large tip angle excitation which may be undesirable in some applications, e.g., DESPOT2 [2], and leads to increased SAR. We propose to use an alternative steady state imaging sequence, referred to as Small-Tip Fast Recovery imaging (STFR) [3], to do water-fat separation and suppress banding artifacts, which works well for flip angles ranging from 16^0 to 90^0. Specifically, this method is based on the gradient crusher based STFR (G-STFR) [4] that is equivalent to the chimera SSFP [5]. The proposed method was demonstrated in phantom and in-vivo experiments on a 3T scanner.

$$\begin{cases} S_1(\boldsymbol{x}) = W(\boldsymbol{x})P_1\big(f_w(\boldsymbol{x})\big) + F(\boldsymbol{x})P_1{}'\big(f_F(\boldsymbol{x})\big) \\ S_2(\boldsymbol{x}) = W(\boldsymbol{x})P_2\big(f_w(\boldsymbol{x})\big) + F(\boldsymbol{x})P_2{}'\big(f_F(\boldsymbol{x})\big) \end{cases} \quad (1)$$

$$\begin{cases} \alpha_1^w(\boldsymbol{x})P_1\big(f_w(\boldsymbol{x})\big) + \alpha_2^w(\boldsymbol{x})P_2\big(f_w(\boldsymbol{x})\big) = 1 \\ \alpha_1^w(\boldsymbol{x})P_1{}'\big(f_F(\boldsymbol{x})\big) + \alpha_2^w(\boldsymbol{x})P_2{}'\big(f_F(\boldsymbol{x})\big) = 0 \end{cases} \quad (2)$$

$$\begin{cases} \alpha_1^F(\boldsymbol{x})P_1\big(f_w(\boldsymbol{x})\big) + \alpha_2^F(\boldsymbol{x})P_2\big(f_w(\boldsymbol{x})\big) = 0 \\ \alpha_1^F(\boldsymbol{x})P_1{}'\big(f_F(\boldsymbol{x})\big) + \alpha_2^F(\boldsymbol{x})P_2{}'\big(f_F(\boldsymbol{x})\big) = 1 \end{cases} \quad (3)$$

$$\begin{cases} W(\boldsymbol{x}) = \alpha_1^W(\boldsymbol{x})S_1(\boldsymbol{x}) + \alpha_2^W(\boldsymbol{x})S_2(\boldsymbol{x}) \\ F(\boldsymbol{x}) = \alpha_1^F(\boldsymbol{x})S_1(\boldsymbol{x}) + \alpha_2^F(\boldsymbol{x})S_2(\boldsymbol{x}) \end{cases} \quad (4)$$

$$\begin{bmatrix} \alpha_1^w(\boldsymbol{x}) \\ \alpha_2^w(\boldsymbol{x}) \end{bmatrix} = \left\| \begin{bmatrix} 1 \\ 0 \end{bmatrix} - \begin{bmatrix} P_1(f_w(\boldsymbol{x})) & P_2(f_w(\boldsymbol{x})) \\ P_1{}'(f_F(\boldsymbol{x})) & P_2{}'(f_F(\boldsymbol{x})) \end{bmatrix} \begin{bmatrix} \alpha_1^w \\ \alpha_2^w \end{bmatrix} \right\|_2^2 \quad (5)$$

Theory: Similar to [1], the proposed method works by linearly combining two phase-cycled acquisitions with B_0 map acquired separately. The noiseless signals of the two acquisitions are modeled in the image domain as in (1), where $S_1(\boldsymbol{x})$ and $S_2(\boldsymbol{x})$ are pixel values of the two acquisitions at location $\boldsymbol{x}$, $W(\boldsymbol{x})$ and $F(\boldsymbol{x})$ are the transverse magnetizations of water and fat respectively, $P_i(\cdot)$ and $P_i{}'(\cdot)$ are signal profiles of the *ith* acquisition in terms of $f_w(\boldsymbol{x})$ and $f_F(\boldsymbol{x})$ which are the offset frequencies of water and fat respectively, e.g., $f_F(\boldsymbol{x}) = f_w(\boldsymbol{x}) - 440$ Hz at 3T. $P_i(\cdot)$ and $P_i{}'(\cdot)$ are both normalized so that the tissue contrast is preserved in $W(\boldsymbol{x})$ and $F(\boldsymbol{x})$; $P_i(\cdot)$ and $P_i{}'(\cdot)$ are centered around water and fat center frequencies respectively, and they are not exactly the same as each other due to large difference of T_1; however, it will be shown that $P_i(\cdot)$ and $P_i{}'(\cdot)$ are relatively insensitive to T_1, T_2 values within their own reasonable ranges. Since $P_i(\cdot)$ and $P_i{}'(\cdot)$ can be determined based on imaging parameters and our G-STFR signal model accurately [4], there is no approximation necessary for $P_i(\cdot)$ and $P_i{}'(\cdot)$, unlike the sinusoidal assumption in [1]. Calculations of the linear combination weights $\alpha_i^w(\boldsymbol{x})$ and $\alpha_i^F(\boldsymbol{x})$, which are used for separation of water and fat respectively, are described in (2) and (3). The water or fat image is then calculated as in (4). Note that both the tip-down and the tip-up pulses are the same regular selective or hard excitation pulses. Empirically, we found that the profiles are insensitive to flip angles ranging from 16^0 to 90^0 which cover the optimal values for most applications.

For each experiment, a lookup table has to be built for $P_i(\cdot)$ and $P_i{}'(\cdot)$ versus offset frequency *f*. We propose an iterative method to calculate $\alpha_i^w(\boldsymbol{x})$ and $\alpha_i^F(\boldsymbol{x})$ as in (5), which is an example for calculating $\alpha_i^w(\boldsymbol{x})$; in (5), absolute values are taken to relax the irrelevant phase of water image, which is a magnitude least square problem [6]. By adjusting the free procession time such that water and fat sit at the peak and the bottom in each magnitude profile, the problem can be manipulated to be very well-conditioned, so regularization is not necessary in (5) to control the magnitude of $\alpha_i^w(\boldsymbol{x})$ and $\alpha_i^F(\boldsymbol{x})$. Furthermore, since the signal profiles are calculated assuming infinite narrow spectra of each component in the voxel, which is not true in practice, we assume Lorentzian-shaped spectra for water and fat which will be convolved with $P_i(\cdot)$ and $P_i{}'(\cdot)$ respectively to produce more realistic signal profiles.

Methods and Results: We first simulated the complex signal profiles, i.e., $P_i(\cdot)$ and $P_i'(\cdot)$, of water and fat produced by G-STFR over ranges of tissue parameters, i.e., $40\text{ ms} \le T_{2,\text{fat}} \le 100\text{ ms}$, $150\text{ ms} \le T_{1,\text{fat}} \le 250\text{ ms}$, $60\text{ ms} \le T_{2,\text{water}} \le 200\text{ ms}$, and $0.6\text{ s} \le T_{1,\text{water}} \le 2\text{ s}$. The results in Fig. 1 demonstrate that the signal profiles are relatively insensitive to different tissue types, so the method can work based on certain uniform tissue parameters.

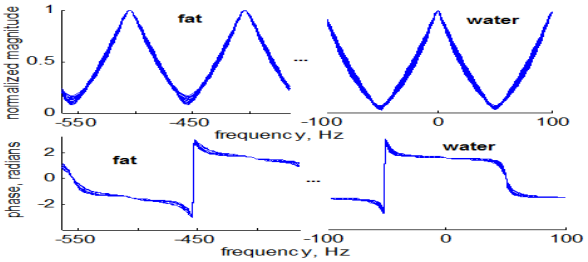

Fig. 1: G-STFR signal profiles for ranges of T_1, T_2 values.

We tested the method in a spherical phantom filled with water ($MnCl_2$ doped) and mineral oil on a 3T GE scanner. The actual T_1, T_2 values are: $T_{1,\text{oil}} \approx 200$ ms, $T_{2,\text{oil}} \approx 22$ ms, $T_{1,\text{water}} \approx 1$ s, $T_{2,\text{water}} \approx 80$ ms. A linear gradient was turned on to generate some B_0 inhomogeneity (-90 ~ 130 Hz). 3D G-STFR was used to acquire $S_1(\boldsymbol{x})$ and $S_2(\boldsymbol{x})$: FOV = 24×24×10 cm, spin-warp readout, 64×64×20 matrix size, $T_R = 8$ ms, $T_E = 3.1$ ms, the free procession time $T_{\text{free}} = 5.4$ ms, flip angles were about 35^0. To demonstrate the robustness of the method to model mismatch, we used inaccurate T_1, T_2 values to calculate $\alpha_i^w(\boldsymbol{x})$ and $\alpha_i^F(\boldsymbol{x})$, i.e., $T_{1,\text{oil}} = 150$ ms, $T_{2,\text{oil}} = 70$ ms, $T_{1,\text{water}} = 2$ s, $T_{2,\text{water}} = 120$ ms. In addition, a bSSFP image with $T_R = 5.38$ ms was acquired for the same object. Fig. 2 shows results from one of the axial slices: The proposed method makes relatively uniform water (on the bottom) and fat (on the top and some attached to the bottom) images without banding artifacts compared to the bSSFP image.

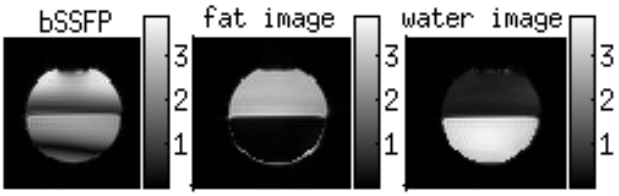

Fig. 2: The phantom experiment result.

Furthermore, the method was tested with the same 3D G-STFR sequence in a human head on the 3T GE scanner. We acquired 3D images of a 4 cm thick axial slab around eyes: FOV = 24×24×10cm, spin-warp readout, 256×256×20 matrix size, $T_R = 10.6$ ms, $T_E = 4.0$ ms, the free procession time $T_{\text{free}} = 8.0$ ms, flip angles are about 20^0. A corresponding bSSFP image with $T_R = 8.0$ ms was acquired. We use uniform tissue parameters for the reconstruction: $T_{1,\text{fat}} = 200$ ms, $T_{2,\text{fat}} = 70$ ms, $T_{1,\text{water}} = 1$ s, $T_{2,\text{water}} = 100$ ms. Fig. 3 shows one of the slices, where the fat (behind eye balls and around skull) and the water image are separated. With a relatively uniform B_0 field, we only observe a small banding artifact in bSSFP (pointed by the red arrow) which is removed by the proposed method. There are still some artifacts in the combined results: the flow-induced artifacts around the through-slab arteries can be reduced by exciting a thicker slab and/or applying flow compensation gradients; moreover, the eye balls are not reconstructed well in both images, which might be due to eye motion between scans.

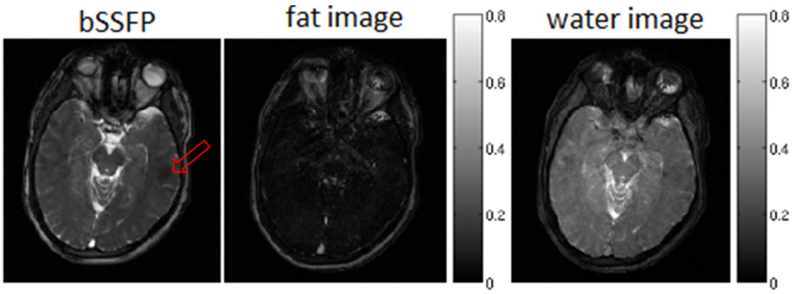

Fig. 3: The in-vivo experiment result.

Conclusions: The proposed method for steady-state water fat separation and banding artifacts suppression is demonstrated at 3T scanners. This steady-state method which works for a wide range of flip angles and T_1, T_2 values can potentially be an alternative to the bSSFP-based method which commonly requires high flip angle and thus high SAR.

References: [1] Quist et al, MRM 2012: 1004-12. [2] Deoni, MRM 2003: 515-26. [3] Nielsen et al., MRM 2012 April. [4] Sun et al., ISMRM 2012: 4183. [5] Bieri et al, ISMRM 2009: 2767. [6] Setsompop et al., MRM, 2008: 908-15. **Acknowledgements:** This work is supported by NIH Grants R01NS58576 and R21EB012674.